

ACSP · Analog Circuits And Signal Processing

Athanasios T. Ramkaj  
Marcel J. M. Pelgrom  
Michiel S. J. Steyaert  
Filip Tavernier

# Multi-Gigahertz Nyquist Analog-to-Digital Converters

Architecture and Circuit Innovations  
in Deep-Scaled CMOS and FinFET  
Technologies

 Springer

# **Analog Circuits and Signal Processing**

## **Series Editors**

Mohammed Ismail, Khalifa University, Dublin, OH, USA

Mohamad Sawan, 18, Shilongshan Road, School of Engineering, Westlake University, Hangzhou, Zhejiang, China

The *Analog Circuits and Signal Processing* book series, formerly known as the *Kluwer International Series in Engineering and Computer Science*, is a high level academic and professional series publishing research on the design and applications of analog integrated circuits and signal processing circuits and systems. Typically per year we publish between 5-15 research monographs, professional books, handbooks, and edited volumes with worldwide distribution to engineers, researchers, educators, and libraries. The book series promotes and expedites the dissemination of new research results and tutorial views in the analog field. There is an exciting and large volume of research activity in the field worldwide. Researchers are striving to bridge the gap between classical analog work and recent advances in very large scale integration (VLSI) technologies with improved analog capabilities. Analog VLSI has been recognized as a major technology for future information processing. Analog work is showing signs of dramatic changes with emphasis on interdisciplinary research efforts combining device/circuit/technology issues. Consequently, new design concepts, strategies and design tools are being unveiled. Topics of interest include: Analog Interface Circuits and Systems; Data converters; Active-RC, switched-capacitor and continuous-time integrated filters; Mixed analog/digital VLSI; Simulation and modeling, mixed-mode simulation; Analog nonlinear and computational circuits and signal processing; Analog Artificial Neural Networks/Artificial Intelligence; Current-mode Signal Processing; Computer-Aided Design (CAD) tools; Analog Design in emerging technologies (Scalable CMOS, BiCMOS, GaAs, heterojunction and floating gate technologies, etc.); Analog Design for Test; Integrated sensors and actuators; Analog Design Automation/Knowledge-based Systems; Analog VLSI cell libraries; Analog product development; RF Front ends, Wireless communications and Microwave Circuits; Analog behavioral modeling, Analog HDL.

Athanasios T. Ramkaj • Marcel J. M. Pelgrom •  
Michiel S. J. Steyaert • Filip Tavernier

# Multi-Gigahertz Nyquist Analog-to-Digital Converters

Architecture and Circuit Innovations in  
Deep-Scaled CMOS and FinFET  
Technologies

 Springer

Athanasios T. Ramkaj  
Stanford University  
Stanford, CA, USA

Marcel J. M. Pelgrom  
Helmond, Noord-Brabant  
The Netherlands

Michiel S. J. Steyaert  
KU Leuven  
Leuven, Belgium

Filip Tavernier  
KU Leuven  
Leuven, Belgium

ISSN 1872-082X                      ISSN 2197-1854 (electronic)  
Analog Circuits and Signal Processing  
ISBN 978-3-031-22708-0              ISBN 978-3-031-22709-7 (eBook)  
<https://doi.org/10.1007/978-3-031-22709-7>

© The Editor(s) (if applicable) and The Author(s), under exclusive license to Springer Nature Switzerland AG 2023

This work is subject to copyright. All rights are solely and exclusively licensed by the Publisher, whether the whole or part of the material is concerned, specifically the rights of translation, reprinting, reuse of illustrations, recitation, broadcasting, reproduction on microfilms or in any other physical way, and transmission or information storage and retrieval, electronic adaptation, computer software, or by similar or dissimilar methodology now known or hereafter developed.

The use of general descriptive names, registered names, trademarks, service marks, etc. in this publication does not imply, even in the absence of a specific statement, that such names are exempt from the relevant protective laws and regulations and therefore free for general use.

The publisher, the authors, and the editors are safe to assume that the advice and information in this book are believed to be true and accurate at the date of publication. Neither the publisher nor the authors or the editors give a warranty, expressed or implied, with respect to the material contained herein or for any errors or omissions that may have been made. The publisher remains neutral with regard to jurisdictional claims in published maps and institutional affiliations.

This Springer imprint is published by the registered company Springer Nature Switzerland AG  
The registered company address is: Gewerbestrasse 11, 6330 Cham, Switzerland

*To Theodor and Linda*

# Preface

The analog-to-digital converter (ADC) is considered the cornerstone of modern electronics due to its fundamental role in virtually any application requiring the transfer of information between the physical (analog) world and the processing (digital) world. This task comes with myriad challenges due to the complex multi-functional ADC nature, further exacerbated when the relevant applications demand stringent performance requirements. Furthermore, bridging the analog and digital worlds fundamentally implies that ADCs must deal with the non-idealities of the former while keeping up with the advancements of the latter.

The rapidly accelerating trend for broader-band signals and software-defined systems has spurred the need for ADCs operating in the multi-GHz sample rate and bandwidth regime. Such converters are highly demanded by applications in the realm of next generation high-speed wireless and wireline communications, automotive radar, and high-end instrumentation, and have attracted a growing attention from both industry and academia. The ever-increasing desire of these systems is to maximize speed, while progressively improving the accuracy and the power efficiency, pushing the performance dimensions to new benchmarks. Meeting these requirements at the multi-GHz regime comes with numerous challenges at the circuit, architecture, and system levels. On top, the constant technology downscaling, dictated by the demand for higher functionality at a reduced power and cost, and the improvement in digital performance, exacerbates these challenges for traditional analog-intensive solutions.

This book follows a holistic approach, from analysis to implementation, to propose innovative circuit, architecture, and system solutions in deep-scaled CMOS and maximize the  $accuracy \cdot speed \div power$  of multi-GHz sample rate and bandwidth ADCs. The approach starts by identifying the major error sources of any practical converter's circuits and quantitatively analyzing their significance on the overall performance, establishing the fundamental accuracy-speed-power limits imposed by circuits, and building an understanding as to what may be achievable from a converter's elementary building blocks. The analysis extends to the architecture level, by introducing a mathematical framework to estimate and compare the accuracy-speed-power limits of high-performance architectures, such as flash, SAR, pipeline,

and pipelined-SAR. To gain insight on the system level and peripheral blocks, a framework is introduced to quantitatively compare interleaver architectures, in terms of achievable bandwidth and sampling accuracy. The strength of the newly introduced frameworks is further enhanced by adding technology effects from four deep-scaled CMOS processes: 65 nm, 40 nm, 28 nm, and 16 nm, building insight into both architecture as well as process choices for optimum performance at given specifications.

The validity of the above holistic approach and the feasibility of the proposed solutions are demonstrated by four prototype ICs, realized in 28 nm bulk CMOS and 16 nm FinFET CMOS:

1. An ultrahigh-speed three-stage triple-latch feed-forward dynamic comparator improves the gain and reduces the delay of dynamic comparators across the entire input range. [28 nm CMOS, presented at *ESSCIRC 2019*, and published in *SSC-L 2019* and *TCAS-I 2022*]
2. A high-speed wide-bandwidth medium resolution single-channel SAR ADC maximizes the  $accuracy \cdot speed \div power$  ratio with a semi-asynchronous timing, an improved bootstrapped input switch, a triple-tail dynamic comparator, and a Unit-Switch-Plus-Cap DAC. [28 nm CMOS, presented at *ESSCIRC 2017*, and published in *JSSC 2018*]
3. A high-resolution wide-bandwidth 8 $\times$ -interleaved hybrid RF ADC with a bufferless input front end, a 3-stage pipelined-SAR sub-ADC, a low excess jitter clock chain, and co-designed analog–digital calibrations significantly improves the state of the art in RF ADCs. [28 nm CMOS, presented at *ISSCC 2019*, and published in *JSSC 2020*]
4. An ultra-wideband highly linear analog front end with a multi-segment distributed attenuation filter and a hybrid amplifier-buffer extends the bandwidth of next-generation direct RF ADC-based receivers to several tens of GHz, enabling direct RF sampling up to mm-wave frequencies. [16 nm FinFET CMOS, presented at *VLSI 2022*, and two US patents]

Stanford, CA, USA  
Helmond, The Netherlands  
Leuven, Belgium  
Leuven, Belgium  
September 2022

Athanasios T. Ramkaj  
Marcel J. M. Pelgrom  
Michiel S. J. Steyaert  
Filip Tavernier

# Acknowledgments

We would like to acknowledge several people and organizations for their valuable contributions to the work in this book.

We thank Boris Murmann (Stanford University, CA, USA), Gabriele Manganaro (MediaTek Inc., MA, USA), Marian Verhelst (KU Leuven, Belgium), and Patrick Wambacq (KU Leuven, Belgium) for their feedback on previous versions of this manuscript and for all the engaging and inspiring discussions throughout the last years. We would also like to acknowledge our collaborators' contributions in the articles discussed throughout this book: Adalberto Cantoni (Analog Devices Inc., MA, USA), Siddharth Devarajan (Analog Devices Inc., MA, USA), Juan Carlos Peña Ramos (ICsense, Leuven, Belgium), and Maarten Strackx (MAGICS Instruments, Geel, Belgium).

Finally, the authors thank Nokia Bell Labs, Antwerp, Belgium, and Analog Devices, Wilmington, MA, USA for their financial support.

# Contents

<b>1</b>	<b>Introduction</b>	1
1.1	Data Converters in a Digital Era: Need and High-Performance Applications	1
1.2	Challenges in Pushing Performance Boundaries	5
1.2.1	ADC Core and Peripherals Challenges	6
1.2.2	The Good, the Bad, and the Ugly of Deep-Scaled CMOS	7
1.3	Research Goal and Objectives	10
1.4	Structure of This Book	12
<b>2</b>	<b>Analog-to-Digital Conversion Fundamentals</b>	15
2.1	Theoretical Background	15
2.1.1	Sampling	16
2.1.2	Ideal Quantization	21
2.2	Error Sources	26
2.2.1	Noise	26
2.2.2	Non-linearity	30
2.2.3	Calibration	33
2.3	Performance Evaluation	34
2.3.1	Metrics	34
2.3.2	Figures of Merit	36
2.4	Accuracy-Speed-Power Limits	37
2.4.1	Sampler Noise Limit	38
2.4.2	Quantizer Noise Limit	41
2.4.3	Metastability Limit	42
2.4.4	Aperture Jitter Limit	47
2.4.5	Mismatch Limit	48
2.4.6	Heisenberg Uncertainty Principle	51
2.4.7	Putting It All Together	53
2.5	Conclusion	54
	Appendix A: Proper FFT Evaluation Setup	55

<b>3</b>	<b>Architectural Considerations for High-Efficiency GHz-Range ADCs</b>	57
3.1	State of the Art	57
3.2	The Flash Architecture	60
3.2.1	Overview	60
3.2.2	Flash Accuracy-Speed-Power Limits	62
3.2.3	Impact of Scaling	65
3.3	The SAR Architecture	69
3.3.1	Overview	69
3.3.2	The DAC in a SAR	70
3.3.3	SAR Accuracy-Speed-Power Limits	78
3.4	The Pipeline Architecture	81
3.4.1	Overview	81
3.4.2	Pipeline Accuracy-Speed-Power Limits	83
3.5	The Pipelined-SAR: A Powerful Hybrid	88
3.5.1	Overview	88
3.5.2	Pipelined-SAR Accuracy-Speed-Power Limits	93
3.6	Architectural Limits' Comparison	98
3.7	Time-Interleaving	102
3.7.1	Overview	102
3.7.2	Interleaving Errors	104
3.7.3	Interleaver Architectures	109
3.8	Conclusion	118
	Appendix B: Transconductance—Settled RA	119
	Appendix C: Transconductance—Integrator RA	120
<b>4</b>	<b>Ultrahigh-Speed High-Sensitivity Dynamic Comparator</b>	121
4.1	Dynamic Regenerative Comparators	121
4.1.1	Single-Stage Latch-Based Strong-ARM Comparator	122
4.1.2	Two-Stage Double-Tail Latched Comparator	125
4.2	Prototype IC: A 28 nm CMOS Three-Stage Triple-Latch Feed-Forward Comparator	128
4.2.1	Circuit Operation and Analysis	128
4.2.2	Simulation and Comparison with Prior Art	133
4.2.3	On-Chip Delay Evaluation Setup	136
4.3	Experimental Verification	137
4.3.1	Measurement Setup	139
4.3.2	Measurement Results	140
4.3.3	State-of-the-Art Comparison	145
4.4	Conclusion	147
<b>5</b>	<b>High-Speed Wide-Bandwidth Single-Channel SAR ADC</b>	149
5.1	Pushing the SAR Conversion Speed	149
5.1.1	Conventional Synchronous Clocking Scheme	150
5.1.2	Speed-Boosting Techniques	151
5.2	Prototype IC: A 1.25 GS/s 7-bit SAR ADC in 28 nm CMOS	156
5.2.1	High-Level Design	156

- 5.2.2 Semi-asynchronous Processing w/o Logic Delay ..... 157
- 5.2.3 Dual-Loop Bootstrapped Input Switch ..... 159
- 5.2.4 Unit-Switch-Plus-Cap DAC ..... 162
- 5.2.5 Triple-Tail Dynamic Comparator ..... 166
- 5.2.6 Custom SAR Logic ..... 171
- 5.3 Experimental Verification..... 173
  - 5.3.1 Measurement Setup ..... 174
  - 5.3.2 Measurement Results ..... 175
  - 5.3.3 State-of-the-Art Comparison ..... 178
- 5.4 Conclusion ..... 179
- 6 High-Resolution Wide-Bandwidth Time-Interleaved RF ADC ..... 183**
  - 6.1 RF Sampling ADCs: Needs and Challenges ..... 183
    - 6.1.1 The ADC Role in the Receiver ..... 184
    - 6.1.2 ADC Architectural Trade-Offs ..... 185
  - 6.2 Prototype IC: A 5 GS/s 12-bit Hybrid TI-ADC in 28 nm CMOS ..... 188
    - 6.2.1 High-Level Design ..... 188
    - 6.2.2 Interleaving Factor and Sub-ADC Architecture ..... 189
    - 6.2.3 Passive Input Front-End ..... 190
    - 6.2.4 Clock Generation and Distribution ..... 194
    - 6.2.5 Hybrid Sub-ADC Design ..... 199
    - 6.2.6 Digital Calibration ..... 203
  - 6.3 Experimental Verification ..... 204
    - 6.3.1 Measurement Setup ..... 205
    - 6.3.2 Measurement Results ..... 207
    - 6.3.3 State-of-the-Art Comparison ..... 213
  - 6.4 Conclusion ..... 214
- Appendix D: TI ADC Power Estimation with On-Chip Input Buffer ..... 216
- 7 Ultra-Wideband Direct RF Receiver Analog Front-End ..... 217**
  - 7.1 Pushing the Bandwidth Beyond 20 GHz ..... 218
    - 7.1.1 Revisiting the Analog Front-End Problem ..... 218
    - 7.1.2 Increasing Integration and Challenges ..... 221
  - 7.2 Prototype IC: A 30 GHz-Bandwidth  $<-57$  dB-IM3 Front-End in 16 nm FinFET CMOS ..... 222
    - 7.2.1 High-Level Front-End Chain ..... 223
    - 7.2.2 Filter with Distributed ESD and Variable Attenuation ..... 224
    - 7.2.3 Two-Path Push-Pull Hybrid Amplifier ..... 230
    - 7.2.4 Push-Pull Bootstrapped Cascoded Buffer ..... 232
  - 7.3 Experimental Verification ..... 236
    - 7.3.1 Measurement Setup ..... 237
    - 7.3.2 Measurement Results ..... 239
    - 7.3.3 State-of-the-Art Comparison ..... 244
  - 7.4 Conclusion ..... 246

<b>8 Conclusions, Contributions, and Future Work</b> .....	247
8.1 Overview and General Conclusions .....	247
8.2 Original Scientific Contributions .....	251
8.3 Suggestions for Future Work .....	254
<b>Bibliography</b> .....	257
<b>Index</b> .....	267

# List of Figures

Fig. 1.1	Illustration of the data conversion as an indispensable bridging function between the real analog world and the digital signal processing world .....	2
Fig. 1.2	Popular ADC applications and architectures covering them .....	3
Fig. 1.3	Wideband ADC-based heterodyne (top left) and zero-IF (top right) vs. direct RF sampling receiver (bottom) .....	4
Fig. 1.4	The three main ADC performance parameters and several factors affecting them on different levels .....	6
Fig. 1.5	CMOS scaling evolution from planar FET to FinFET to GAAFET. Picture credit: Samsung .....	8
Fig. 1.6	Theoretical cut-off frequency versus channel length scaling [10] .....	8
Fig. 1.7	Supply and threshold voltage versus channel length scaling .....	9
Fig. 1.8	BEOL interconnect comparison between 65 nm (left) and 32 nm (right) CMOS processes [11] .....	10
Fig. 2.1	Block diagram of an ideal A/D conversion (top) and the resulting waveforms at every part of the chain (bottom) .....	16
Fig. 2.2	Sampling a continuous-time signal using a Dirac pulse sequence .....	17
Fig. 2.3	Frequency spectrum of a signal multiplied with a sequence of Dirac pulses .....	18
Fig. 2.4	(a) Single-tone signals with different frequencies (b) fall in the same frequency location after spectrum processing .....	18
Fig. 2.5	Dual-sided frequency spectrum highlighting different Nyquist zones .....	19
Fig. 2.6	(a), (b) Two cases of signals with bands meeting the Nyquist criterion and (c) one scenario where bands are overlapping leading to information loss .....	19

Fig. 2.7	Anti-aliasing filter on a parasitic tone when <b>(a)</b> sampling at Nyquist rate (slightly oversampled in practice) and <b>(b)</b> oversampling by $M > 1$ .....	20
Fig. 2.8	Conceptual model and transfer characteristic of an ideal quantizer .....	22
Fig. 2.9	Sawtooth approximation of $\epsilon_q$ as a function of time .....	22
Fig. 2.10	Uniformly distributed PDF of $\epsilon_q$ within $\pm\Delta/2$ .....	23
Fig. 2.11	Frequency spectra of an ideally quantized with various resolutions 77 MHz signal sampled at 1 GS/s ( $N_{\text{FFT}} = 1024$ ) .....	24
Fig. 2.12	Conceptual model of a real converter including error sources from the different blocks .....	26
Fig. 2.13	<b>(a)</b> Simple model of a sampler and <b>(b)</b> its noise spectrum .....	27
Fig. 2.14	<b>(a)</b> Simple quantizer model and <b>(b)</b> its allowed operation time .....	28
Fig. 2.15	<b>(a)</b> Sampler with jitter and <b>(b)</b> time to voltage error translation .....	29
Fig. 2.16	<b>(a)</b> DNL in transfer characteristic with corresponding curve and <b>(b)</b> INL in transfer characteristic with corresponding curve .....	31
Fig. 2.17	Simple sampler model with input termination network .....	39
Fig. 2.18	Fundamental limits due to sampler noise: <b>(a)</b> accuracy-speed and <b>(b)</b> accuracy-power .....	40
Fig. 2.19	Fundamental limits due to quantizer noise: <b>(a)</b> accuracy-speed and <b>(b)</b> accuracy-power .....	43
Fig. 2.20	Quantizer output for a valid (gray) and a metastable (black) case .....	44
Fig. 2.21	Fundamental limits due to metastability of a standalone quantizer: <b>(a)</b> accuracy-speed and <b>(b)</b> accuracy-power .....	46
Fig. 2.22	Simple model for clock power estimation for a certain jitter .....	48
Fig. 2.23	Fundamental limits due to aperture jitter: <b>(a)</b> accuracy-speed and <b>(b)</b> accuracy-power .....	49
Fig. 2.24	Limits imposed by mismatch: <b>(a)</b> accuracy-speed and <b>(b)</b> accuracy-power .....	51
Fig. 2.25	Fundamental accuracy-speed limit due to Heisenberg .....	52
Fig. 2.26	Fundamental limit curves from all the error sources analyzed in this chapter: <b>(a)</b> accuracy-speed and <b>(b)</b> accuracy-power .....	53
Fig. 3.1	State-of-the-art performance of various ADC architectures with data points taken from [36] <b>(a)</b> accuracy-speed and <b>(b)</b> accuracy-energy .....	58
Fig. 3.2	Block diagram of a B-bit flash ADC (the S/H is optional) .....	60
Fig. 3.3	Simplified small-signal model of an NMOS transistor (bulk is omitted for simplicity) .....	66

Fig. 3.4	$f_T$ vs. $g_m/I_D$ and $f_T \cdot g_m/I_D$ vs. $g_m/I_D$ in four CMOS processes .....	67
Fig. 3.5	Flash accuracy-speed-power limits: (a) for different $f_s$ in 28 nm and (b) at $f_s = 4$ GHz in the processes under comparison .....	68
Fig. 3.6	Block diagram of a $B$ -bit SAR ADC .....	69
Fig. 3.7	(a) Scale equivalent of a binary SA algorithm and (b) waveform operation in the voltage vs. time domain .....	71
Fig. 3.8	3-bit example of the conventional CDAC switching scheme. $V_{REF}$ is annotated as $V_R$ to preserve clarity due to space constraints .....	72
Fig. 3.9	3-bit example of the split-capacitor CDAC switching scheme. $V_{REF}$ is annotated as $V_R$ to preserve clarity due to space constraints .....	73
Fig. 3.10	3-bit example of the energy-saving CDAC switching scheme. $V_{REF}$ is annotated as $V_R$ to preserve clarity due to space constraints .....	74
Fig. 3.11	3-bit example of the monotonic CDAC switching scheme. $V_{REF}$ is annotated as $V_R$ to preserve clarity due to space constraints .....	75
Fig. 3.12	3-bit example of the MCS CDAC switching scheme. $V_{REF}$ is annotated as $V_R$ to preserve clarity due to space constraints .....	76
Fig. 3.13	Switching energy for the different CDAC switching schemes .....	77
Fig. 3.14	SAR accuracy-speed-power limits: (a) for different $f_s$ in 28 nm and (b) for $f_s = 500$ MHz in the processes under comparison .....	80
Fig. 3.15	Block diagram of a $B$ -bit $m$ -stages pipeline ADC .....	81
Fig. 3.16	Residue plot of stage- $s$ : (a) ideal case with $A_s = 2^{B_s}$ , (b) $A_s = 2^{B_s}$ with error and no OR, and (c) $A_s = 2^{B_s-1}$ with error and $2\times$ -OR .....	82
Fig. 3.17	Basic $g_m - C$ amplifier for modeling the RA gain stage .....	84
Fig. 3.18	Pipeline with 1,2,3,4-bit/stage effective resolution accuracy-speed-power limits in 28 nm: (a) $f_s = 500$ kHz, (b) $f_s = 500$ MHz, and (c) $f_s = 1.3$ GHz .....	89
Fig. 3.19	Pipeline accuracy-speed-power limits across different processes at $f_s = 500$ MHz: (a) 1-bit/stage, (b) 2-bit/stage, and (c) 3-bit/stage .....	90
Fig. 3.20	Block diagram of a $B$ -bit two-stage pipelined-SAR ADC .....	91
Fig. 3.21	Illustration of conversion energy requirement in (a) a binary SAR ADC and (b) a two-stage pipelined-SAR ADC .....	92

Fig. 3.22	2,3,4,5-stage pipelined-SAR with accuracy-speed-power limits in 28 nm: <b>(a)</b> $f_s = 500$ kHz, <b>(b)</b> $f_s = 500$ MHz, and <b>(c)</b> $f_s = 1.3$ GHz .....	96
Fig. 3.23	Pipelined-SAR accuracy-speed-power limits across different processes at $f_s = 500$ MHz: <b>(a)</b> three-stage, <b>(b)</b> four-stage, and <b>(c)</b> five-stage .....	97
Fig. 3.24	Accuracy-speed-power limits for the different ADC architectures studied at $f_s = 500$ kHz .....	99
Fig. 3.25	Accuracy-speed-power limits for the different ADC architectures studied at $f_s = 500$ MHz .....	100
Fig. 3.26	Accuracy-speed-power limits for the different ADC architectures studied at $f_s = 1.3$ GHz .....	101
Fig. 3.27	<b>(a)</b> High-level block diagram of an $N$ -channel TI-ADC and <b>(b)</b> sampling of a signal using an $N$ -interleaved Dirac pulse sequence .....	103
Fig. 3.28	Power vs. frequency illustration of a non-TI- and a TI-ADC .....	103
Fig. 3.29	Illustration of mismatch errors in a four-channel TI-ADC example .....	105
Fig. 3.30	Graphical illustration of sub-ADC offset mismatch errors in a four-channel TI-ADC: <b>(a)</b> time waveform and <b>(b)</b> frequency spectrum .....	105
Fig. 3.31	Graphical illustration of sub-ADC gain mismatch errors in a four-channel TI-ADC: <b>(a)</b> time waveform and <b>(b)</b> frequency spectrum .....	106
Fig. 3.32	Graphical illustration of sub-ADC timing mismatch errors in a four-channel TI-ADC: <b>(a)</b> time waveform and <b>(b)</b> frequency spectrum .....	107
Fig. 3.33	Graphical illustration of sub-ADC bandwidth mismatch errors in a four-channel TI-ADC: <b>(a)</b> time waveform and <b>(b)</b> frequency spectrum .....	108
Fig. 3.34	Simulated SNDR vs. <b>(a)</b> $\sigma_{OS}/V_{DD}$ , <b>(b)</b> $\sigma_G/G$ , <b>(c)</b> $\sigma_{\Delta T}/T_s$ , <b>(d)</b> $\sigma_{BW}/BW$ , and <b>(e)</b> $\sigma_{BW}/BW$ with separated gain/phase and <b>(f)</b> combined errors .....	110
Fig. 3.35	Classification tree for different interleaver architectures .....	110
Fig. 3.36	<b>(a)</b> Direct interleaver architecture and timing diagram for $N = 8$ <b>(b)</b> with 50% duty-cycle clocks and <b>(c)</b> with (1/8)-100% duty-cycle clocks .....	111
Fig. 3.37	<b>(a)</b> Interleaver architecture with a hierarchical $N = L \times K$ de-multiplexing and <b>(b)</b> timing diagram for $N = 8$ with $L \times K = 2 \times 4$ .....	112
Fig. 3.38	<b>(a)</b> Interleaver architecture with $N = L \times K$ re-sampling hierarchy and <b>(b)</b> timing diagram for $N = 8$ with $L \times K = 2 \times 4$ .....	113

Fig. 3.39	Equivalent $RC$ model for (a) interleaver and (b) simple switch .....	114
Fig. 3.40	Bandwidth vs. channel count for different interleavers in (a) 65 nm, (b) 40 nm, (c) 28 nm, and (d) 16 nm CMOS .....	115
Fig. 3.41	Sampling accuracy vs. channel count for the interleavers in 28 nm at (a) $Nf_s = 2.5$ GHz, (b) $Nf_s = 5.0$ GHz, (c) $Nf_s = 7.5$ GHz, and (d) $Nf_s = 10$ GHz .....	117
Fig. 4.1	Single-stage strong-ARM comparator and its signal waveforms .....	122
Fig. 4.2	Double-tail comparator and its signal waveforms .....	126
Fig. 4.3	Proposed three-stage TLFF dynamic comparator .....	129
Fig. 4.4	LTV representation of the proposed TLFF comparator .....	130
Fig. 4.5	Simulated timing waveforms of the proposed TLFF comparator .....	134
Fig. 4.6	Simulated outputs and delay versus $\Delta V_I$ for different comparators .....	135
Fig. 4.7	Top-level diagram of the multiple comparators test chip .....	137
Fig. 4.8	Die photo of the 28 nm IC with zoomed-in comparator layout views .....	138
Fig. 4.9	Measurement setup of the multiple comparators test chip with the prototype 13.5 Gb/s TLFF comparator .....	139
Fig. 4.10	Measured CLK-OUT delays for the TLFF, SAC, and DTC comparators versus (a) $\Delta V_I$ , (b) $V_{CM}$ , and (c) $V_{DD}$ .....	141
Fig. 4.11	Measured noise cumulative distribution and Gaussian distribution fitting curve for (a) the SAC, (b) the DTC, (c) the TLFF, and (d) measured input-referred noise vs. $V_{CM}$ .....	143
Fig. 4.12	Measured (a) energy consumption of the TLFF, SAC, and DTC versus $V_{DD}$ and (b) energy-delay product versus $V_{DD}$ .....	144
Fig. 4.13	(a) Measured $\Delta V_I$ eye, (b) measured bathtub curve of the TLFF, (c) measured CLK eye, and (d) measured OUT eye .....	145
Fig. 5.1	Timing sequence illustration of a $B$ -bit SAR with a conventional synchronous clocking scheme .....	150
Fig. 5.2	Timing sequence illustration of a $B$ -bit SAR with an internally asynchronous clocking scheme .....	151
Fig. 5.3	Timing sequence illustration of a $B$ -bit SAR with a multi-bit per cycle resolving scheme (2-bit per cycle shown in the example) .....	153
Fig. 5.4	Timing sequence illustration of a $B$ -bit SAR with multiple comparators loop unrolling clocking scheme .....	153
Fig. 5.5	Timing sequence illustration of a $B$ -bit SAR with extra cycles and redundancy implemented (one extra cycle shown in the example) .....	155
Fig. 5.6	Top-level architecture of the proposed ADC and its timing diagram .....	157

Fig. 5.7	Implemented semi-asynchronous scheme with the logic delay eliminated from the critical path .....	158
Fig. 5.8	Typical bootstrap circuit with its speed critical loop highlighted .....	159
Fig. 5.9	Improved dual-loop bootstrap circuit proposed in this work .....	160
Fig. 5.10	(a) Timing illustration and (b) simulated $M_S$ on-resistance for the typical and the proposed bootstrap circuit .....	161
Fig. 5.11	DAC topology with a constant $V_{CM}$ and $C_H$ to set the signal range .....	162
Fig. 5.12	Schematic and simulated settling time of (a) a conventional UC CDAC and (b) the proposed USPC CDAC .....	164
Fig. 5.13	Single-ended partial layout of the USPC CDAC (the actual implementation is differential) .....	165
Fig. 5.14	Schematic of the implemented triple-tail dynamic comparator .....	166
Fig. 5.15	Simulated performance of the triple-tail comparator .....	167
Fig. 5.16	Simulated outputs of the triple-tail comparator (top) and one of the logic memory latches (bottom) .....	168
Fig. 5.17	(a) Simulated comparator resolving time and (b) input-referred noise versus $V_{CM,I}$ and (c) resolving time and (d) energy versus $\Delta V_I$ .....	170
Fig. 5.18	Custom SAR logic including the comparator clock, bit phases, and memory elements .....	171
Fig. 5.19	Schematic of one memory cell with optimized critical path toward the CDAC reference switches (top). Timing diagram and truth table of the memory cell (bottom) .....	172
Fig. 5.20	Die micrograph of the 28 nm IC with a zoomed-in view of the SAR core occupying an active area of $0.0071 \text{ mm}^2$ .....	173
Fig. 5.21	Measurement setup of the 1.25 GS/s 7-bit SAR prototype .....	174
Fig. 5.22	Measured static performance with the histogram (code density) test at 1.25 GS/s for a sinusoidal input of 160 kHz: (a) DNL and (b) INL .....	176
Fig. 5.23	Measured output spectra at 1.25 GS/s for (a) a Nyquist input frequency and (b) an $8\times$ Nyquist input frequency .....	177
Fig. 5.24	Measured SFDR/SNDR versus (a) input frequency at 1.25 GS/s and (b) sample rate for a 76 MHz input .....	178
Fig. 5.25	Measured FoM versus (a) input frequency at 1.25 GS/s and (b) sample rate for a 76 MHz input .....	179
Fig. 6.1	Generic block diagram of a direct RF sampling receiver .....	184
Fig. 6.2	Sub-ADC and interleaving overhead vs. channel count illustration .....	186
Fig. 6.3	Major design strategies regarding the choice of the sub-ADC and the interleaving factor .....	186

Fig. 6.4	Accuracy-speed standings of the ADCs adopting the two design strategies. Points taken from [36] .....	187
Fig. 6.5	Top-level diagram of the complete 5 GS/s 12-bit TI-ADC architecture (single-ended shown for simplicity) .....	189
Fig. 6.6	Passive front-end model of this ADC (single-ended shown) .....	190
Fig. 6.7	(a) Bootstrap circuit employed for $S_{IN}$ and (b) timing waveforms of the important nodes .....	192
Fig. 6.8	Proposed intertwined input/clock Y-tree structure to minimize the front-end loading .....	192
Fig. 6.9	Simulated (a) S-parameters and (b) input impedance of this front-end .....	194
Fig. 6.10	Input current profile of this front-end for (a) 300 MHz and (b) 2.4 GHz input frequencies .....	195
Fig. 6.11	Simulated HD2 vs. differential input-clock coupling (unbalancing) for a near-2.5 GHz input .....	195
Fig. 6.12	Timing diagram with the generated clocks of the TI-ADC .....	196
Fig. 6.13	(a) Simulated SNR vs. $\sigma_{\text{jitter}}$ and (b) SFDR vs. $\sigma_{\text{skew}}$ at Nyquist .....	196
Fig. 6.14	Block diagram of the proposed clock conditioning chain for this ADC .....	197
Fig. 6.15	(a) DDT circuit with simulated (b) sampling edge skew and tuning range and (c) capacitance spread of one DDT unit cell .....	198
Fig. 6.16	Detailed block diagram of the implemented 12-bit three-stage pipelined-SAR sub-ADC .....	200
Fig. 6.17	Dynamic integrator RA with simulated $SAR_1$ - $SAR_2$ residue .....	201
Fig. 6.18	Sub-ADC internal asynchronous timing sequence with re-timing .....	202
Fig. 6.19	One slice top-level diagram of the $8\times$ synthesized correction block .....	203
Fig. 6.20	Die micrograph of the 28 nm complete IC with a sub-ADC layout view occupying a core area of $0.015 \text{ mm}^2$ .....	205
Fig. 6.21	Measurement setup of the 12-bit 5 GS/s TI ADC prototype (top). Photo of the overall setup (bottom-left). Closer view of the motherboard with the four-layer Rogers 4350 chip board mounted on its center through high-speed Samtec connectors (bottom-right). The bare die is placed in a plated cavity .....	206
Fig. 6.22	Measured (black solid curve) and simulated (gray dotted curve) ADC transfer characteristic showing a bandwidth in excess of 6 GHz .....	208
Fig. 6.23	Measured calibrated output spectra at 5 GS/s for (a) 75 MHz, (b) 2.4 GHz, and (c) 4.8 GHz input frequencies .....	209

Fig. 6.24	Measured SFDR/SNDR versus <b>(a)</b> input frequency at 5 GS/s and <b>(b)</b> sample rate for a 2.4 GHz input .....	210
Fig. 6.25	Measured static performance at 5 GS/s for a sinusoidal input of 7.4 MHz: <b>(a)</b> DNL and <b>(b)</b> INL .....	211
Fig. 6.26	Measured output spectrum at 5 GS/s for a $-6.1$ dBFS two-tone input signal at 74.5 MHz 81.7 MHz .....	212
Fig. 6.27	Measured output spectrum at 5 GS/s for a $-6.4$ dBFS two-tone input signal at 1.67 GHz 1.85 GHz .....	212
Fig. 6.28	Measured power partitioning versus sample rate for a 2.4 GHz .....	213
Fig. 6.29	FoM <sub>S</sub> comparison with relevant SotA RF ADCs [36] .....	213
Fig. 7.1	Two chip-to-substrate illustrations: <b>(a)</b> flip-chip through copper pillars and <b>(b)</b> wire bonding through gold bondwires .....	220
Fig. 7.2	Buffered front-end model including on-chip/interface/off-chip contributions (single-ended shown) .....	220
Fig. 7.3	Simulated S-parameters of the front-end model, gradually adding the contributions: <b>(a)</b> $S_{21}$ and <b>(b)</b> $S_{11}$ .....	221
Fig. 7.4	Top-level block diagram of the proposed front-end (single-ended shown for simplicity) .....	223
Fig. 7.5	<b>(a)</b> Ideal ninth-order Chebyshev filter with its component values for two $R_T$ values and <b>(b)</b> simulated S-parameters and group delay .....	226
Fig. 7.6	Implementation of the proposed filter with the distributed ESD and variable attenuation (single-ended shown) .....	226
Fig. 7.7	Attenuator cells employed in this work: <b>(a)</b> $\Pi$ -cell, <b>(b)</b> T-cell, and <b>(c)</b> their resistance values rounded to include multiple matched units .....	227
Fig. 7.8	Simulated bandwidth (relative) and linearity of the two attenuator cells for the different attenuation settings: <b>(a)</b> 1 dB, <b>(b)</b> 2 dB, and <b>(c)</b> 4 dB .....	228
Fig. 7.9	Simulated S-parameters of the implemented filter across the different attenuation settings: <b>(a)</b> $S_{21}$ and <b>(b)</b> $S_{11}$ .....	229
Fig. 7.10	Simulated filter two-tone IM3 vs. frequency for the best (0 dB) and worst (11 dB) attenuation settings .....	230
Fig. 7.11	Proposed push-pull hybrid CG-CS amplifier with resistive source degeneration and series-shunt peaking .....	231
Fig. 7.12	Push-pull buffer with two-level bootstrapped cascoding .....	233
Fig. 7.13	Simulated amplifier-buffer transfer characteristic for a capacitive load and the implemented matched load .....	234
Fig. 7.14	Simulated two-tone IM3 vs. frequency of the amplifier-buffer chain .....	234
Fig. 7.15	AC-noise simulation of the amplifier-buffer chain with 300 fF load .....	235

Fig. 7.16 Simulated two-tone IM3 vs. frequency of the complete front-end chain for three different load cases ..... 236

Fig. 7.17 Die micrograph of the 16 nm FinFET IC with front-end occupying a core area of about 0.15 mm<sup>2</sup> ..... 237

Fig. 7.18 Measurement setup of the 30 GHz bandwidth front-end prototype ..... 238

Fig. 7.19 Measured front-end small-signal performance for different attenuation settings and six samples ..... 240

Fig. 7.20 Measured one-tone output spectra for (a) 2.5 GHz and (b) 5 GHz input frequencies and (c) measured HD2/HD3 vs. input frequency ..... 241

Fig. 7.21 Measured two-tone spectra at 5 and 20 GHz for 0 dB (left) and 11 dB (right) attenuation settings ..... 242

Fig. 7.22 Measured two-tone IM3 for six samples vs. (a) carrier frequency and (b) tone spacing ..... 242

Fig. 7.23 Measured constellations and spectra at 5 GHz frequency for (a) 1024-QAM and (b) 2048-QAM signals ..... 243

Fig. 7.24 Measured EVM and ACLR vs. frequency for 1024-QAM and 2048-QAM modulated signals ..... 244

# List of Tables

Table 2.1	Comparison between calculated and simulated SQNR for different $B$ .....	25
Table 2.2	Typical process parameters and comparison with $kT$ .....	50
Table 3.1	Core supply voltage and simulated minimum capacitance in four deep-scaled CMOS processes .....	65
Table 3.2	Bit partitioning for different aggregate resolutions in a 2,3,4,5-stage pipelined-SAR including 2 $\times$ -OR between stages ....	93
Table 4.1	Summary of the TLFF, SAC, and DTC on the same test chip.....	146
Table 4.2	TLFF comparison with state-of-the-art comparators .....	146
Table 5.1	Performance summary and comparison with state-of-the-art SAR ADCs .....	180
Table 6.1	RA gain variation with temperature (typical-typical corner).....	202
Table 6.2	Performance summary and comparison with state-of-the-art wideband TI RF ADCs.....	215
Table 7.1	Performance summary and comparison with state-of-the-art ADC-based receiver front-ends.....	245

# Chapter 1

## Introduction



Real-world phenomena comprise to their vast majority analog quantities; that is continuous-time and continuous-amplitude signals able to take any value at any particular instant. However, manipulation and storage of data are mainly performed in the digital domain due to several benefits of digital signal processing, such as reduced sensitivity to noise and distortion, increased flexibility and reconfigurability, and continuous performance improvement with technology scaling. As a result, Analog-to-Digital (A/D) conversion performed by an Analog-to-Digital Converter (ADC) and Digital-to-Analog (D/A) conversion performed by a Digital-to-Analog Converter (DAC) are indispensable operations in almost all electronic systems.

This introductory chapter starts by briefly outlining the need and applicability of data converters in a digital era, in Sect. 1.1. Key high-performance ADC applications are briefly discussed. Section 1.2 introduces challenges in simultaneously improving the three main ADC performance parameters. These come on a circuit level, an architectural level, a system level, and a technology level, with the last one being particularly important as it affects the other three. The main scope of the research described in this book and its objectives are listed and briefly discussed in Sect. 1.3. Finally, Sect. 1.4 concludes this chapter with the structural organization of this book.

### 1.1 Data Converters in a Digital Era: Need and High-Performance Applications

Electronic devices undeniably play a crucial role in tremendously improving every aspect of our modern life: from massive communication and transportation infrastructure to personalized entertainment systems and healthcare. To a great extent, this level of accessibility to electronic devices and services owes to the expansion of Digital Signal Processing (DSP), leading to a progressively digital electronic world. The fundamental reason for the DSP advances finds its root

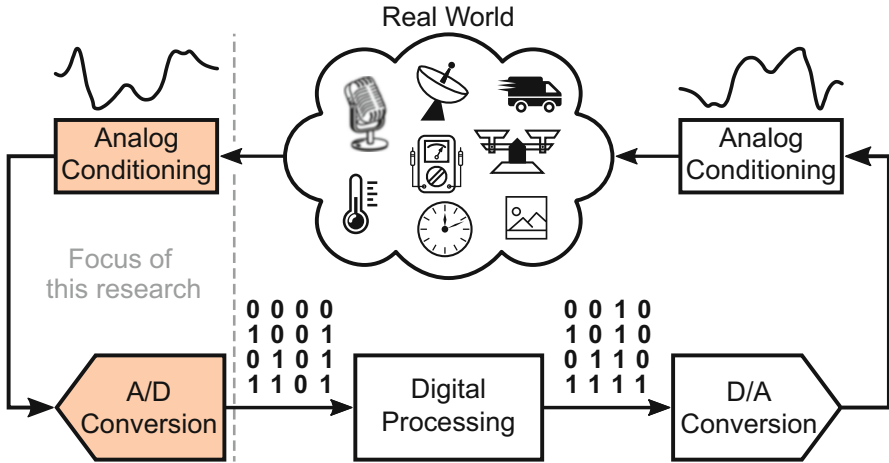


**Fig. 1.1** Illustration of the data conversion as an indispensable bridging function between the real analog world and the digital signal processing world

in the down-scaling and integration advantages of Very Large Scale Integration (VLSI) technologies, offering a higher functionality per unit area for a reduced power and cost. Following Gordon E. Moore's law proposed in 1965 [1], the number of devices per chip doubles every roughly 2 years, with an even higher rate recently [2]. Further, digital circuits offer several advantages with respect to their analog equivalents, such as reduced susceptibility to distortion and noise, less dependency on process-voltage-temperature variations, increased flexibility and reconfigurability, and an unprecedented ability to perform complex computations on-demand, making Systems-on-a-Chip (SoC)s the norm.

Yet, real-world phenomena comprise analog quantities, such as velocity, volume, weight, temperature, voltage, current, etc. Therefore, A/D conversion is a vital function in most electronic devices, to provide the translation interface between the physical and electronic worlds, as illustrated in Fig. 1.1. Similarly, D/A conversion enables the interaction of the device with the environment and the humans, who perceive and process data in the form of analog quantities. Even without the human in the loop, the information exchange between two devices still requires conversion of the data from the digital domain to the analog domain and back. At the transmit side, the digital data is converted into the analog domain to travel through a certain medium. Equivalently, at the receive side, the signal comes either in an analog form or in a degraded by the medium digital form; therefore, it is processed as analog information before it is converted into the digital domain. This role of data converters as interfaces between the analog and digital domains puts them in a unique position in the signal processing chain but also poses considerable design challenges since they must deliver an equivalent or better performance than the corresponding digital systems. For the ADC in particular, which is the focus of this work, to maximally leverage the favorable properties of DSP, its function should be

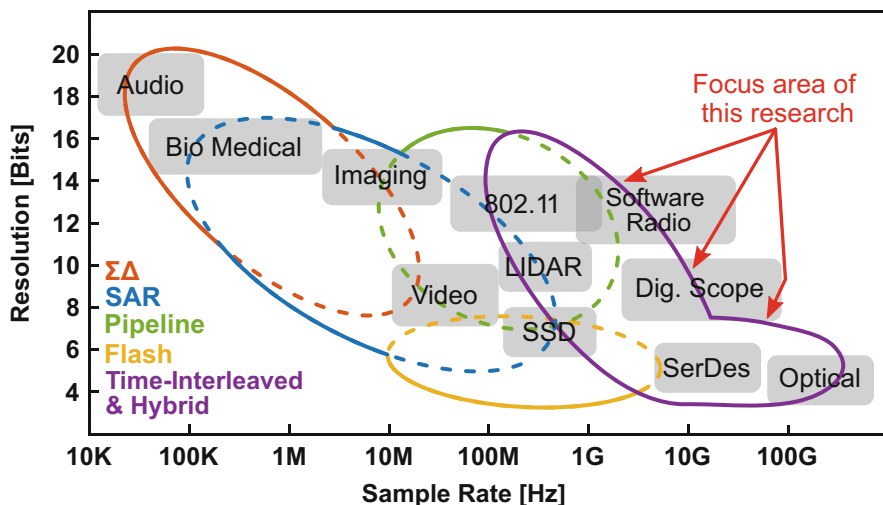
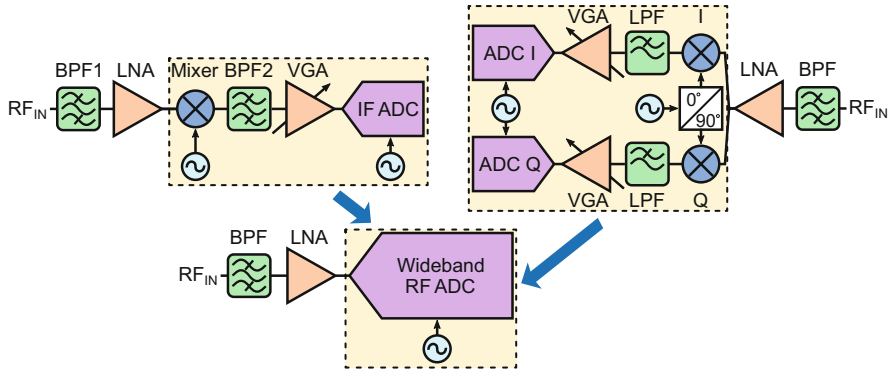


Fig. 1.2 Popular ADC applications and architectures covering them

performed as early as possible in the chain. However, to account for additional and unpredictable signal corruption by the medium, one or more analog conditioning blocks usually precede the converter, whose design is added on the existing set of challenges.

ADCs are employed in a vast and constantly growing number of applications incorporating DSP, either standalone or integrated on the same die or substrate with other blocks composing a larger complex system. More often than not, the performance of the ADC determines the overall performance of the system it is included in. The various applications span a wide range of needs and specifications, including healthcare (diagnostic imaging), consumer electronics (mobile phones, audio, video), automotive (RADAR, LIDAR), next-generation communications (wireline, wireless, optical), and high-end measurement/instrumentation (digital storage oscilloscopes). Some noteworthy applications with established as well as under development specifications are illustrated in Fig. 1.2. To try and meet the demands of such applications, different ADC architectures have been developed. The most widely used up to date are flash, pipeline, Successive Approximation Register (SAR), and sigma-delta ( $\Sigma\Delta$ ). These topologies all have their merits and drawbacks in terms of different specifications, such as sample rate (speed), bandwidth, aggregate resolution, effective resolution (actual), noise, linearity, power consumption, complexity, scalability, etc., making them better tailored for some applications than others. However, as depicted in the conceptual illustration of Fig. 1.2, overlapping target areas exist, such that more than one application can be satisfied by several architectures. To extend the sample rate beyond that of a single converter, time-interleaving has been extensively applied to the above architectures. More recently, hybrid converters have emerged, combining the merits of different



**Fig. 1.3** Wideband ADC-based heterodyne (top left) and zero-IF (top right) vs. direct RF sampling receiver (bottom)

architectures,<sup>1</sup> to extend the range of achievable performance and keep up with the rapidly advancing number/demands of future applications.

Undeniably, the field that has established data converters as a hot research topic in both industry and academia for several decades now is that of communications [3]. The constantly increasing demand for higher bandwidth and accuracy in wireline and wireless communication systems is majorly driving the advances in research and development of ADCs, as being key blocks in every receiver. The multi-band requirements of fifth-generation (5G) and future sixth-generation (6G) cellular mobile networks [4] and data over cable networks [5] call for ADCs with high resolution (10–12 bits), multi-GS/s sample rates (5 GS/s or higher), and several GHz of signal bandwidth (half the sample rate or more) while ensuring high linearity (60–70 dB) and low power (preferably below 500 mW). Realizing such ADCs and integrating them with the digital processor in deep-scaled Complementary Metal-Oxide-Semiconductor (CMOS) empower the direct RF sampling receiver topology [6], depicted in Fig. 1.3. This is the closest hardware equivalent to the ideal Software-Defined Radio (SDR) [7]. By leveraging the advanced DSP capabilities in finer CMOS processes, this topology simplifies the analog signal chain and captures multiple bands with a reduced receiver count, lowering area and cost, with improved flexibility and efficiency.

On another high-speed communications front, the rapid emergence of cloud computing and the Internet-of-Things (IoT) has dramatically increased the demand for a higher bandwidth in data center infrastructures. Consequently, the data rates of the transceivers in these systems have reached numbers as high as 112 Gb/s, with future plans to extend to 224 Gb/s and beyond. With Pulse-Amplitude Modulation (PAM-4) currently the prevailing signaling method, for an ADC-based receiver,

<sup>1</sup> One of the proposed prototypes Integrated Circuit (IC)s in this book is a hybrid converter of such kind.

this translates to sample rate requirements of 56 GS/s (112 Gb/s) and a theoretical<sup>2</sup> 112 GS/s (224 Gb/s) with 6–8-bit resolution. To keep up with these sample rates, suitable ADCs are typically realized with a massive amount of time-interleaving ( $\geq 64$ , rarely  $\geq 36$ ) [8, 9]. However, this significantly increases the power and area, on top of deteriorating the signal bandwidth due the large input loading. Further, time-interleaving results in offset, gain, timing, and bandwidth mismatches between the different sub-ADCs, which deteriorate accuracy and require complex calibration schemes, further increasing power and complexity. It is of great interest to develop speed-boosting techniques to increase the sub-ADC sample rate (beyond 1 GS/s), such that the aforementioned interleaving-associated drawbacks are reduced while ensuring negligible accuracy degradation as well as minimizing the power and complexity. Again, to maximally exploit the DSP benefits in advanced CMOS nodes, it is favorable to place the ADC on the same chip; therefore, scalable-friendly solutions are highly desirable.

The above applications require very-high-performance multi-GHz ADCs on multiple specifications and are key drivers for future performance advancements. It is important to note that these specifications are highly desirable to enable next-generation communications, but not entirely achievable.<sup>3</sup> As such, they were used to motivate this work in extending the limits beyond what is realizable.

## 1.2 Challenges in Pushing Performance Boundaries

The previous section briefly discussed some common ADC specifications and requirements for key multi-GHz-range applications. Generally, many different metrics exist, with different importance depending on the target application. However, in a generalized manner, three main parameters encompass the overall ADC performance in a nutshell; these are accuracy, speed, and power. Under accuracy, we include metrics such as aggregate/effective resolution, dynamic range, noise, and linearity. With speed, we denote both sample rate and bandwidth, in the sense that if one increases, the other one must follow. These three main parameters, as illustrated in Fig. 1.4, are bound to each other and influenced by several factors on different levels, such as on a circuit level, an architectural level, a system level, and a technological/process level. These factors present considerable challenges in all the levels, making it non-trivial (even impossible) to simultaneously push all three parameters toward the desired directions, especially at multi-GHz sample rate and bandwidth.

---

<sup>2</sup> This is one of the potential future options under consideration with several others being investigated, such as PAM-6 or a different signaling method altogether.

<sup>3</sup> At the time of this writing, these applications are undergoing research and prototyping phases to determine viability and long-term reliability.